Electronic Supplementary Information (ESI)

Nitrogen-doped porous carbon nanosheets as a robust catalyst for tunable CO_2 electroreduction to syngas

Jiaojiao Gui,[a] Kaifu Zhang,*[a] Xiaowen Zhan,[b] Yu Yu,[a] Tao Huang,[a] Yunkai Li,[a] Jingyu Xue,[a] Xin Jin,[a] Shan Gao*[a] and Yi Xie[c]

[a.]College of Chemistry and Chemical Engineering, Anhui University, Hefei, Anhui 230601 P. R. China.

[b.]School of Materials Science and Engineering, Anhui University, Hefei, Anhui 230601 P. R. China.

[c.]Hefei National Laboratory for Physical Sciences at Microscale, University of Science & Technology of China, Hefei, Anhui 230026 P. R. China.

*Corresponding authors.

E-mail: shangao@ahu.edu.cn, kfzhang@ahu.edu.cn

1. Experimental

1.1 CO_2 Reduction Procedure

The reduction process was performed using a conventional three-electrode electrochemical H-type cell, with a piece of Nafion®117 membrane as a separator. An Ag/AgCl and a Pt foil (1×1 cm) were used as the reference and the counter electrodes, respectively. A 30 mL 1.0 M $KHCO_3$ solution was used as the electrolyte, which was bubbled with 1.0 atm CO_2 (99.999%) to reach saturation with CO_2.

All potentials initially measured in this work were converted to the reversible hydrogen electrode (RHE) using the following Nernst equation:

$$E(RHE) = E(Ag/AgCl) + 0.199 + 0.059 \times pH$$

The Faradaic efficiency of CO was calculated from the total amount of charge (Q/C) passed through the sample and the total amount of CO (nCO/mol). $Q=I\times t$, where I is the reduction current at a specific applied potential, and t is the time for the constant reduction current. The total amount of CO produced was measured using gas chromatography (GC, Agilent 8860). As two electrons are needed to produce one CO molecule, the Faradaic efficiency can be calculated as follows: Faradaic efficiency = $2F\times nCO/(I\times t)$, where F is the Faraday constant (96,485 C/mol).

1.2 Electrochemically Active Surface Area (ECSA) Measurement

The ECSA was estimated by measuring the capacitive current associated with double-layer charging from the scan rate dependence of cyclic voltammetry (CV). The measurement was performed among a potential window of -0.041 to 0.158 V vs. RHE, where the Faradaic current on working electrode is negligible.

1.3 *In-situ* FTIR.

The preparation of working electrodes for operando IR measurements were modified from a previously reported method. Briefly, an Au thin film is plated on the reflective surface of the Si prism, and then drop-coated with the catalyst ink. The catalyst ink was prepared by mixing 5 mg samples with 30 μL Nafion (5%) in 0.5 mL deionized water. The ink dispersion was then uniformly drop-coated onto the above prepared Au film. The working electrode was mounted in a one-compartment, three-electrode spectroelectrochemical cell with a platinum-wire as the counter electrode and a standard Ag/AgCl electrode as the reference. A bare Au film without catalyst loading was served as the background control. The FTIR spectra were captured using a Nicolet iS50 FT-IR spectrometer equipped with a MCT detector. The spectral resolution was set to 4 cm^{-1} for all measurements. All electrochemical tests were controlled using a CHI electrochemical workstation (CHI760E) with 1.0 M $KHCO_3$ used as the electrolyte. Before the measurements, Ar gas was bubbled into the

electrolyte for at least 20 min to remove the residual air, followed by a continuous CO_2 purge for at least 30 min until the electrolyte is CO_2-saturation. In a typical test, with CO_2 continuously bubbled into the electrolyte, the activation of the working electrode was first carried out by cycling the potential between 0 and -1.0 V vs. RHE until a repeatable CV was obtained. Then, the potential was swept between -0.3 and -0.7 V vs. RHE at 5 mV s^{-1} for electrochemical measurements.

2. Addition Data

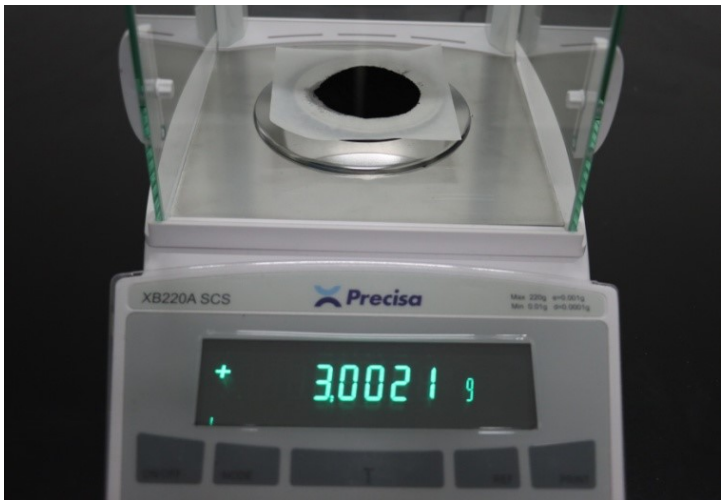

Fig. S1 The digital image for the sample of NCN-6.

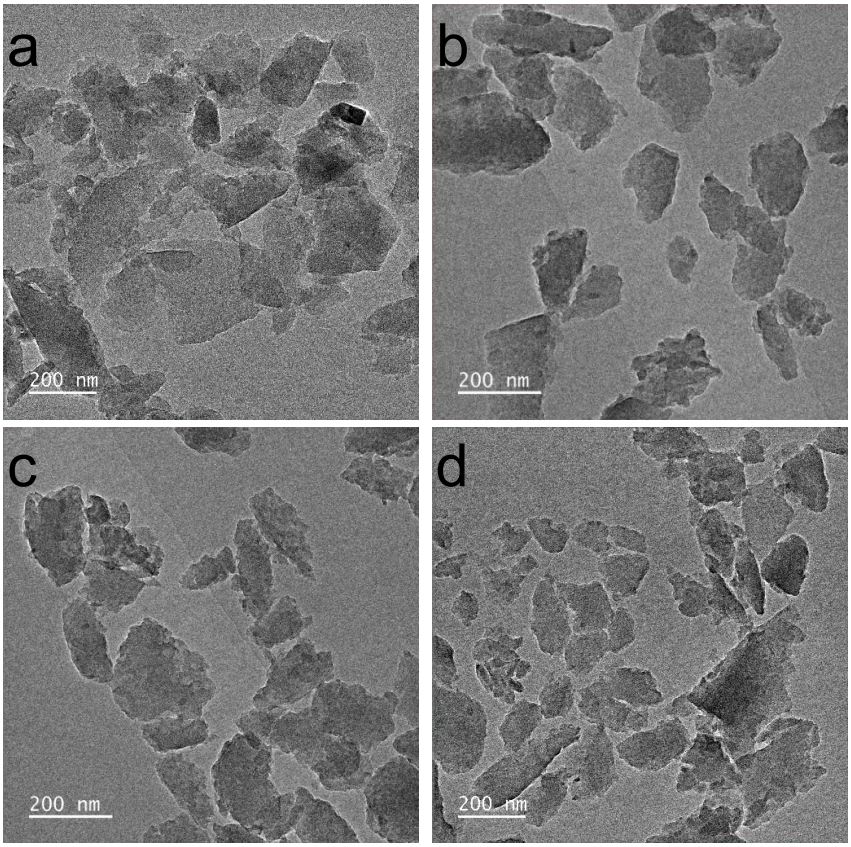

Fig. S2 TEM images of samples: (a) NCN. (b) NCN-3. (c) NCN-4.5. (d) NCN-9.

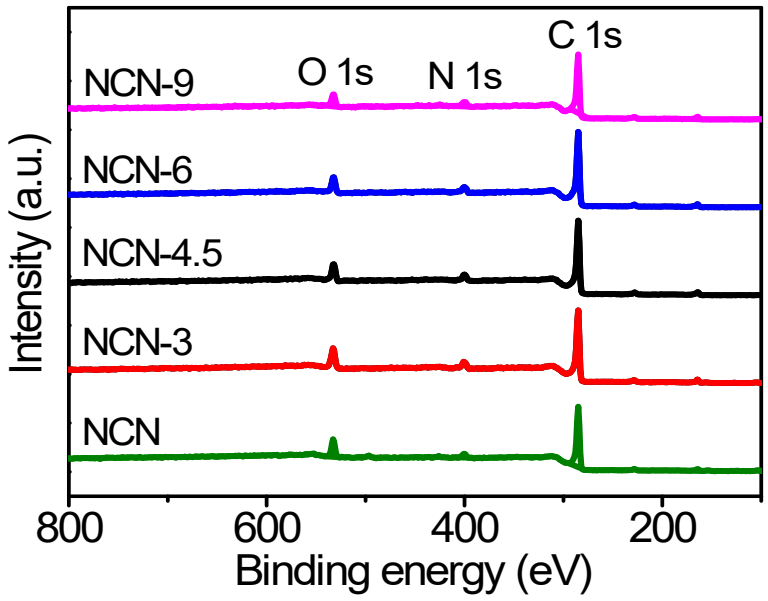

Fig. S3 The XPS survey of all prepared NCN materials.

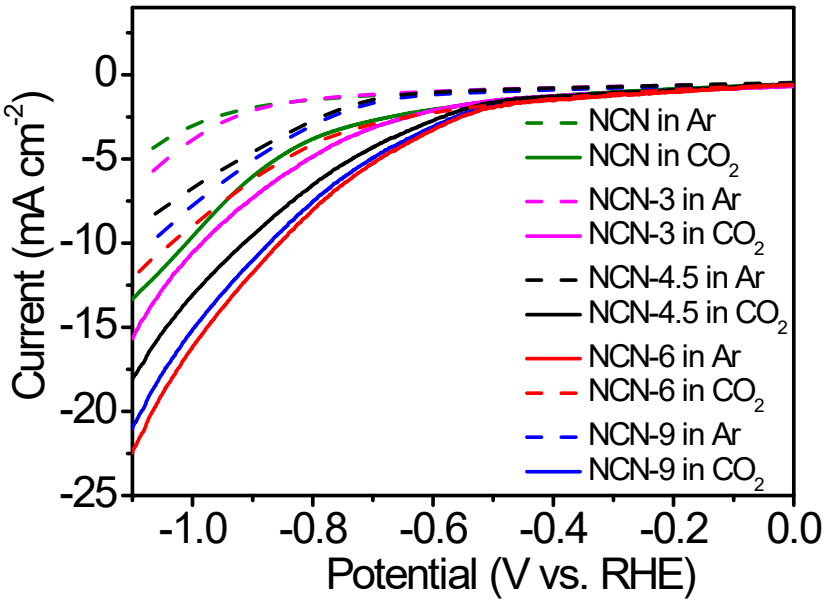

Fig. S4 LSV curves of all as-prepared NCN materials in CO_2-saturated (solid line) and Ar-saturated (dashed line) 1 M $KHCO_3$ solution.

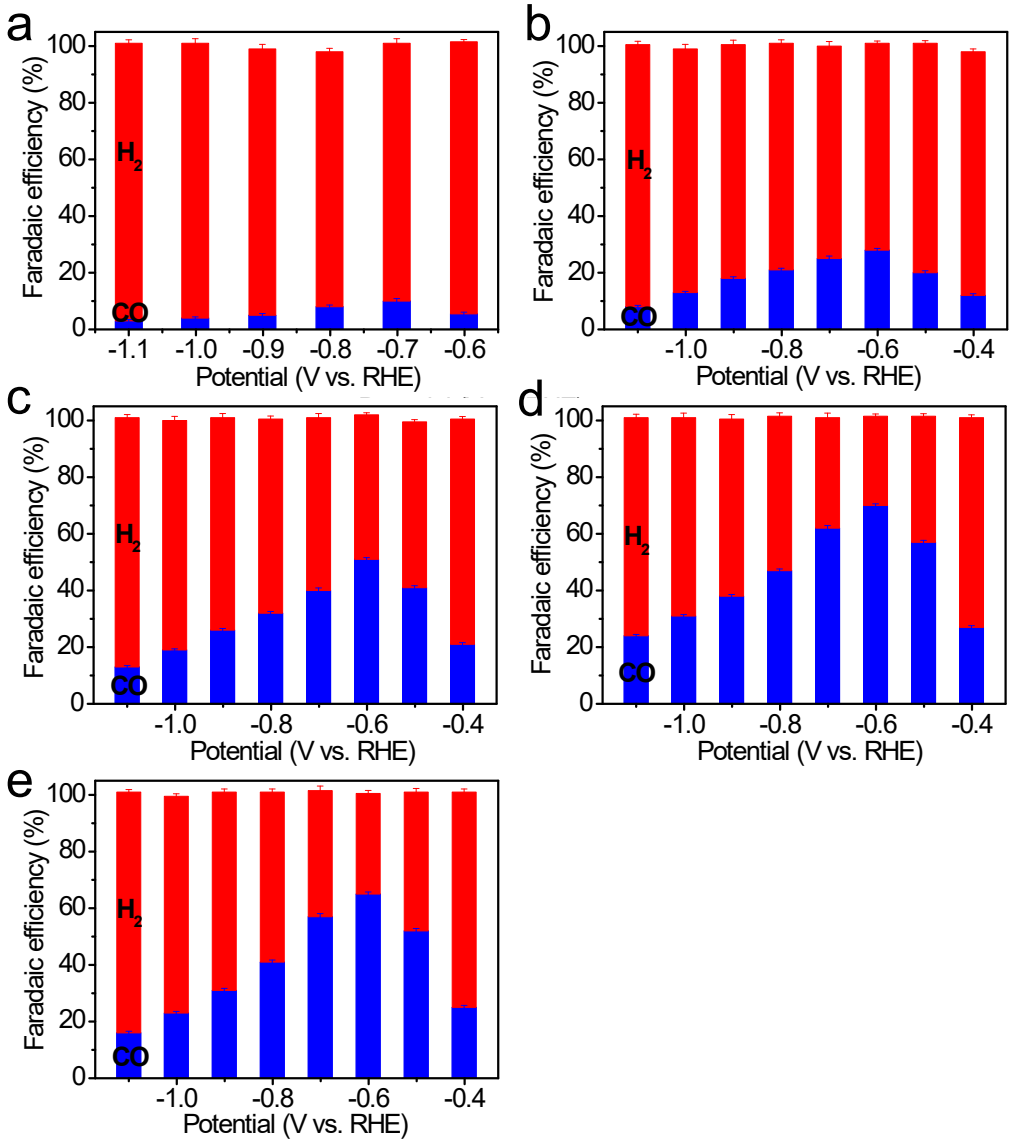

Fig. S5 FE of CO_2 and H_2 distribution depending on applied potential:(a) NCN. (b) NCN-3. (c) NCN-4.5. (d) NCN-6. (e) NCN-9.

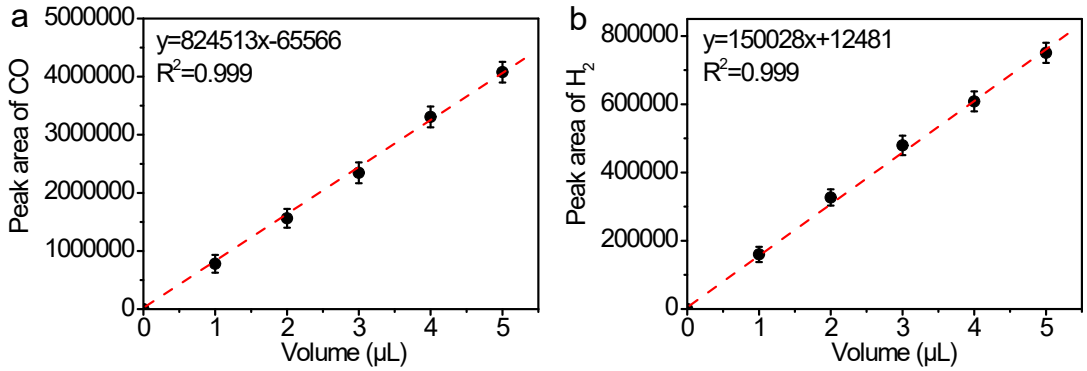

Fig. S6 The relevant standard curve for the detection of (a) CO and (b) H_2 products.

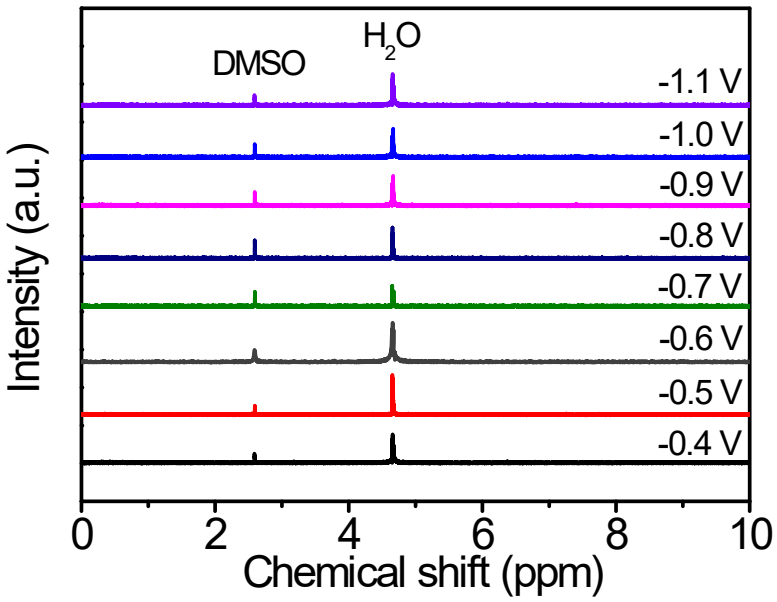

Fig. S7 NMR of liquid products of NCN-6 at each potential from -0.4 V to -1.1 V vs. RHE.

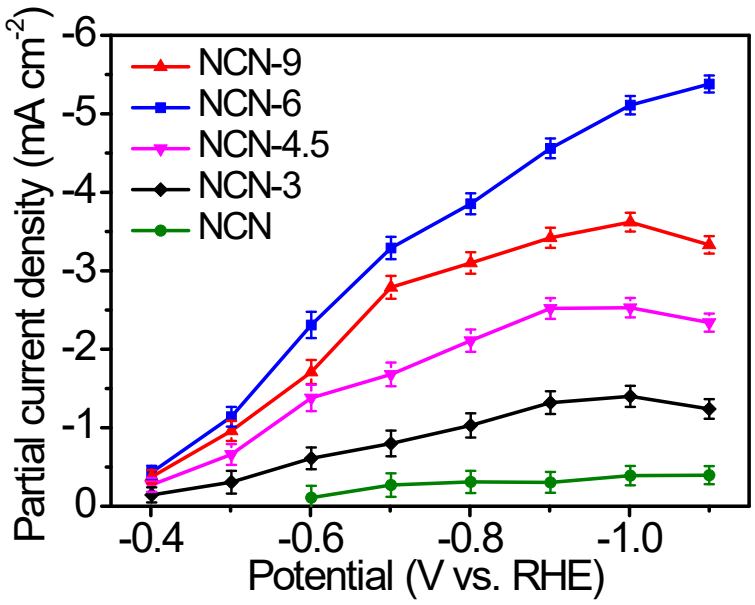

Fig. S8 Partial current density of CO generated on various NCN materials.

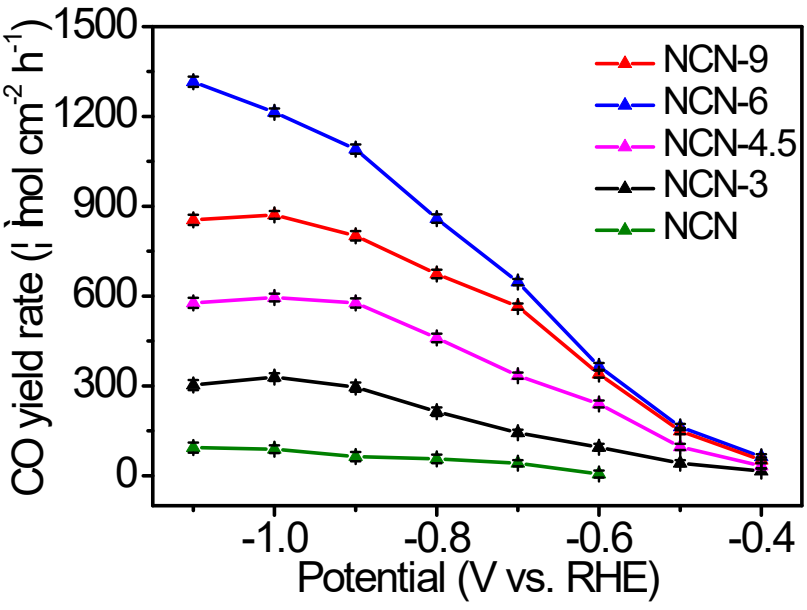

Fig. S9 CO production rate over various NCN catalysts at the given potentials.

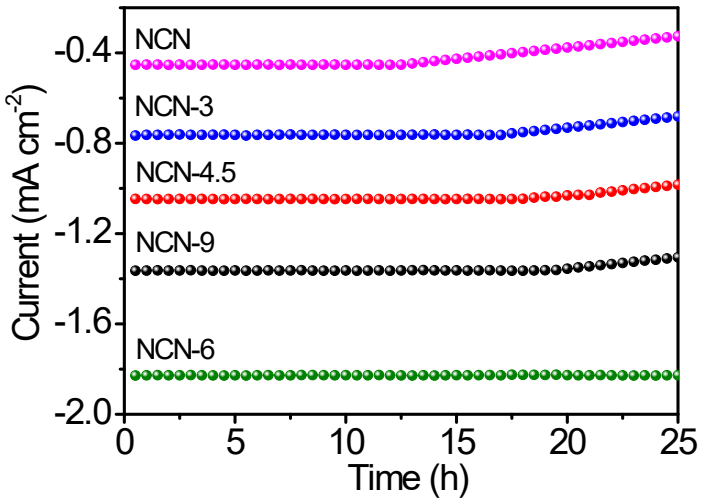

Fig. S10 Long-term stability of all as-prepared catalysts in 1.0 M $KHCO_3$ at the -0.6V vs. RHE.

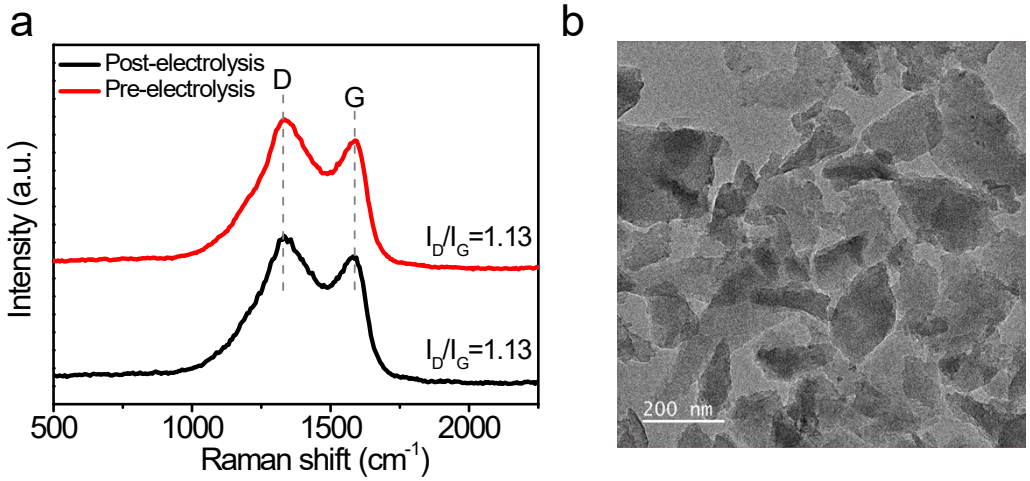

Fig. S11 (a) Raman spectra and (b) TEM image of NCN-6 after CO_2RR at -0.6 V vs. RHE over 25 h.

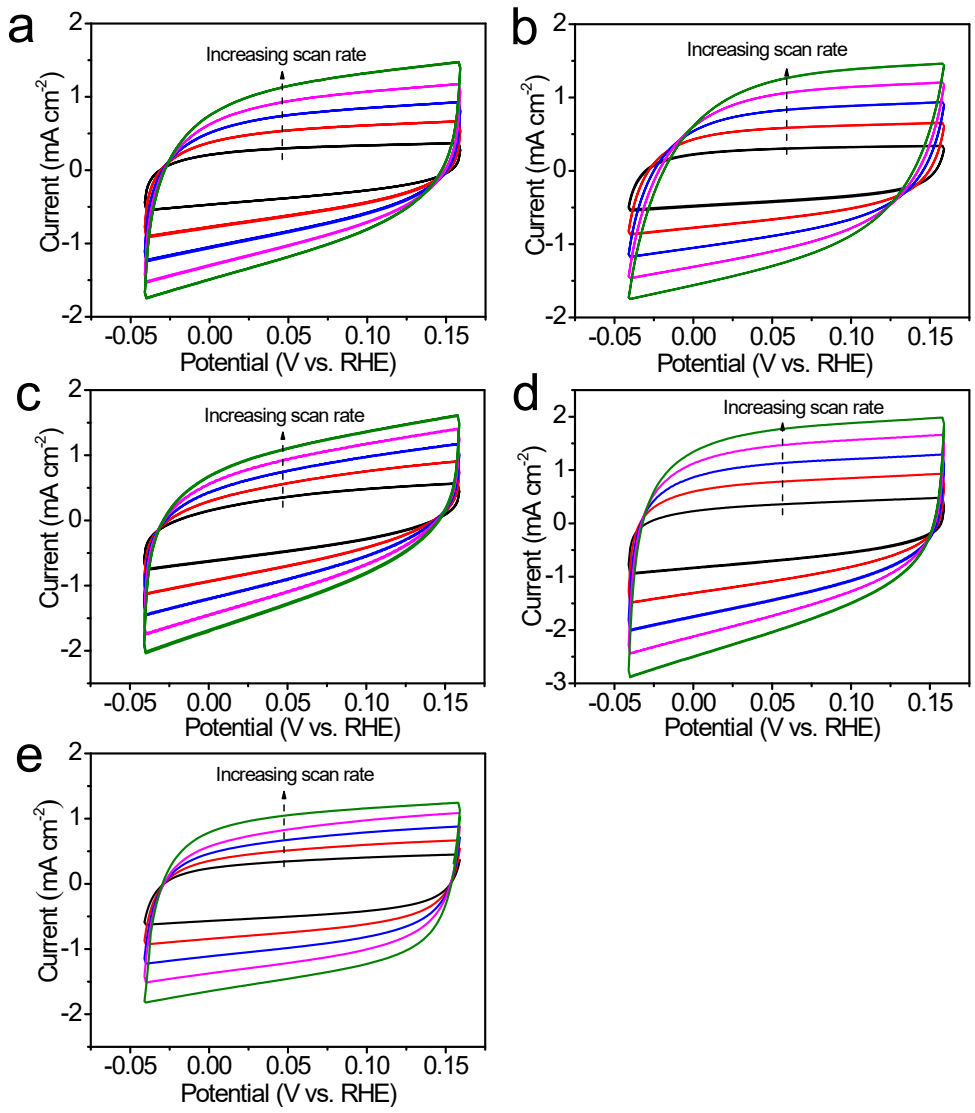

Fig. S12 Current density plots against potentials under a series scan rates of (a) NCN. (b) NCN-3. (c) NCN-4.5. (d) NCN-6. (e) NCN-9. Electrolyte: 1 M $KHCO_3$. The scan rate: 10, 20, 30, 40 and 50 mV s^{-1}.

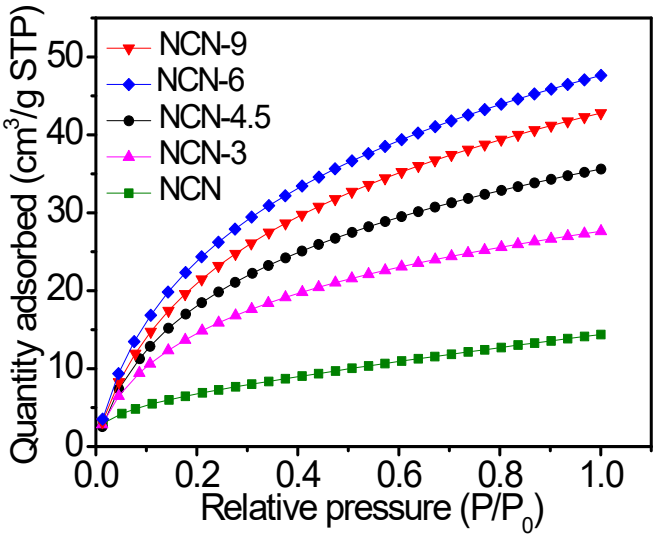

Fig. S13 CO_2 adsorption isotherms of various NCN catalysts.

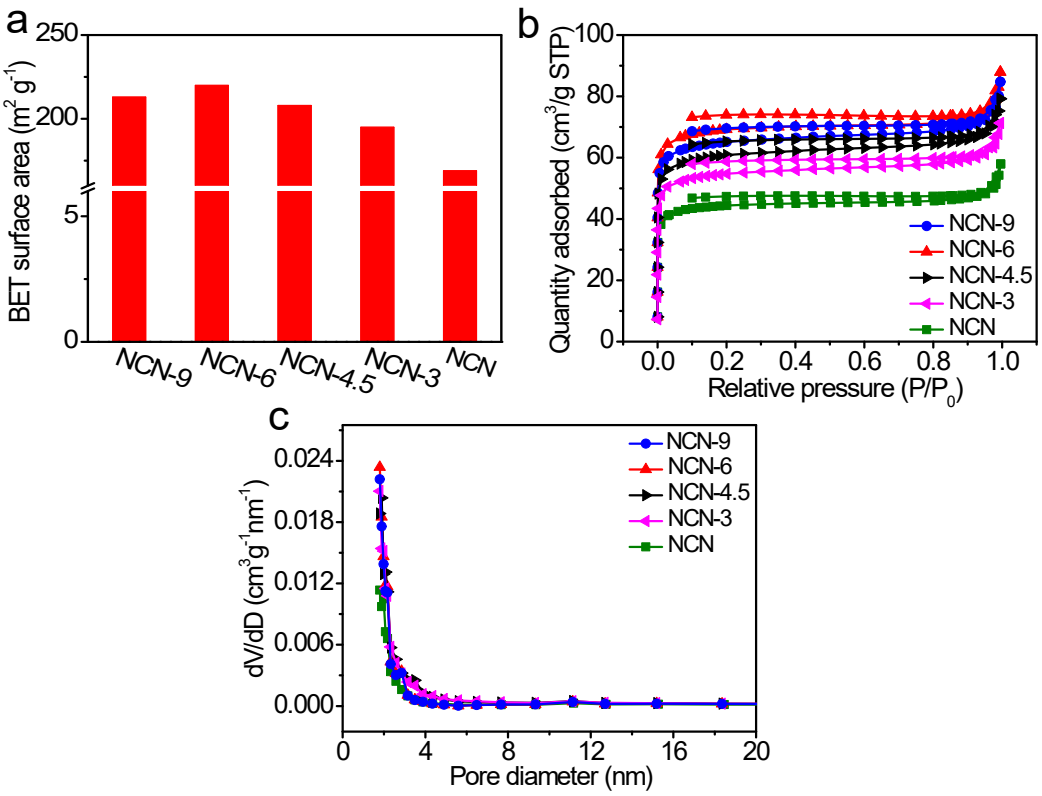

Fig. S14 (a) The BET surface areas, (b) the adsorption-desorption and (c) pore size distribution isotherms of NCN, NCN-3, NCN-4.5, NCN-6 and NCN-9.

Table S1. The content of N and C in different catalysts by elemental analysis.

Catalysts	The content C/Atom%	The content N/Atom%
NCN	95.8	4.1
NCN-3	94.3	5.7
NCN-4.5	93.2	6.8
NCN-6	92.3	7.7
NCN-9	92.6	7.4

Table S2. The content of N species in different catalysts by XPS.

Catalysts	Pyridinic N /Atom%	Pyrrolic N /Atom%	Graphitic N /Atom%	Oxidized N /Atom%
NCN	0.44	0.55	2.12	0.57
NCN-3	0.88	0.61	2.28	1.27
NCN-4.5	1.37	0.68	2.81	1.08
NCN-6	1.74	0.75	2.82	1.28
NCN-9	1.67	0.77	2.77	1.14

Table S3. Electrocatalytic CO_2 RR performance of recently reported metal-free catalysts.

Catalysts	Electrolyte	FE_{CO}	Current density (mA cm $^{-2}$)	Ref.
NCN-6	1.0M $KHCO_3$	70%	-22	This work
NSHCF900	0.1M $KHCO_3$	94%	-103	1
OA-PCN	0.5M$NaHCO_3$	40%	-7	2
MPC-1000	0.1M $KHCO_3$	62%	-6	3
NPC-1000	0.5M $KHCO_3$	98.4%	-14	4
Se-CNs	0.1M $KHCO_3$	90%	-20	5
NS-CNSs-1000	0.5M $KHCO_3$	85.4%	-18	6
NS-C-900	0.1M $KHCO_3$	92%	-14	7
NC-1100	0.5M $KHCO_3$	95%	-12	8
NCNT	0.1M $KHCO_3$	80%	-1.0	9
NC-900-HH	0.1M $KHCO_3$	90%	-5	10

References

1 H. Yang, Y. Wu, Q. Lin, L. Fan, X. Chai, Q. Zhang, J. Liu, C. He and Z. Lin, Composition tailoring via N and S co-doping and structure tuning by constructing hierarchical pores: Metal-free catalysts for high-performance electrochemical reduction of CO_2, *Angew. Chem. Int. Ed*., 2018, **57**, 15476-15480.

2 N. Meng, W. Zhou, Y. Yu, Y. Liu and B. Zhang, Superficial hydroxyl and amino groups synergistically active polymeric carbon nitride for CO_2 electro-reduction, *ACS Catal.*, 2019, **9**, 10983-10989.

3 F. Pan, A. Liang, Y. Duan, Q. Liu, J. Zhang and Y. Li, Self-growth-templating synthesis of 3D N, P, Co-doped mesoporous carbon frameworks for efficient bifunctional oxygen and carbon dioxide electroreduction, *J. Mater. Chem. A*, 2017, **5**, 13104-13111.

4 D. Xue, H. Xia, W. Yan, J. Zhang and S. Mu, Defect engineering on carbon-based catalysts for electrocatalytic CO_2 reduction, *Joule*, 2018, **2**, 2551-2582.

5 B. Zhang, J. Zhang, F. Zhang, L. Zheng, G. Mo, B. Han and G. Yang, Selenium-doped hierarchically porous carbon nanosheets as an efficient metal-free electrocatalyst for CO_2 reduction, *Adv. Funct. Mater.*, 2020, **30**, 1906194.

6 G. Wang, M. Liu, J. Jia, H. Xu, B. Zhao, K. Lai, C. Tu and Z. Wen,

Nitrogen and sulfur co-doped carbon nanosheets for electrochemical reduction of CO_2, *ChemCatChem*, 2020, **1**, 2203-2208.

7 F. Pan, B. Li, W. Deng, Z. Du, Y. Gang, G. Wang and Y. Li, Promoting electrocatalytic CO_2 reduction on nitrogen-doped carbon with sulfur addition, *Appl. Catal. B-Environ.*, 2019, **252**, 240-249.

8 Z. Zhang, L. Yu, Y. Tu, R. Chen, L. Wu, J. Zhu and D. Deng, Unveiling the active site of metal-free nitrogen-doped carbon for electrocatalytic carbon dioxide reduction, *Cell Rep. Phys. Sci.*, 2020, **1**, 100145.

9 J. Wu, R. Yadav, M. Liu, P. Sharma, C. Tiwary, L. Ma, X. Zou, X. Zhou, B. Yakobson, J. Lou and P. Ajayan, Achieving highly efficient, selective, and stable CO_2 reduction on nitrogen-doped carbon nanotubes, *ACS Nano*, 2015, **9**, 5364-5371.

10 P. Yao, Y. Qiu, T. Zhang, P. Su, X. Li and H. Zhang, N-doped nanoporous carbon from biomass as a highly efficient electrocatalyst for the CO_2 reduction reaction, *ACS Sustain. Chem. Eng.*, 2019, **7**, 5249-5255.